
DRAFT

CMS Paper

The content of this note is intended for CMS internal use and distribution only

2009/11/05

Archive Id: 1.7

Archive Date: 2009/11/02 14:16:18

Evidence for a Massive Narrow Resonance in the di-Lepton Mass Spectra in CMS

The CMS Collaboration

Abstract

Evidence for a narrow resonance has been found by the CMS Collaboration in the e^+e^- and $\mu^+\mu^-$ channels. The data correspond to 50 pb^{-1} of pp collisions at 10 TeV provided by the CERN LHC. The significance of the peak in the e^+e^- channel is 3.9σ , and in the $\mu^+\mu^-$ channel, 4.9σ . When combined, and taking systematic uncertainties into account, the significance is 6.2σ . The measured mass of the resonance is $M_{\ell\ell} = 1.24 \pm 0.15 \pm 0.04 \text{ TeV}$, and the effective cross section is $\sigma \times B(pp \rightarrow X \rightarrow \ell^+\ell^-) = 21 \pm 3 \pm 2 \text{ pb}$.

This box is only visible in draft mode. Please make sure the values below make sense.

PDFAuthor:	Michael Schmitt, Claire Shepherd-Themistocleous
PDFTitle:	Evidence for a Massive Narrow Resonance in the di-Lepton Mass Spectra in CMS
PDFSubject:	PHYSICS
PDFKeywords:	CMS, PHYSICS, DILEPTON, RESONANCE

Please also verify that the abstract does not use any user defined symbols

1 Introduction

Many models of new physics predict the existence of a narrow resonance at the TeV mass scale, decaying with substantial branching ratios to charged lepton pairs. Theoretical details can be found in numerous reviews [1].

CMS is a multi-purpose collider detector located at point 5 of the LHC at CERN [2]. Tracking is provided by silicon strip detectors and an inner pixel detector. A crystal calorimeter (ECAL) measures accurately the energy of electron and photon showers. A hadron calorimeter (HCAL) measures the energies of hadrons outside the ECAL. Both the ECAL and the HCAL are finely segmented and cover both the barrel and endcap regions. A superconducting solenoidal coil placed outside the calorimetry provides a uniform field of 3.8 T. Drift tubes track muons in the barrel region outside the coil, and cathode strip chambers track them in the endcaps. Resistive plate chambers add redundancy to the muon tracking, and a fast trigger signal. All detector systems were in good working order, similar to the performance established with cosmic rays [3].

The data used for this letter were recorded in 2010 when the LHC was delivering pp collisions at a center-of-mass energy of 10 TeV. The trigger system provides highly efficient triggers for electrons and muons with $E_T > 20$ GeV and $p_T > 20$ GeV, respectively [4]. A sample of 37 million electron triggers and 22 million muon triggers was analyzed, corresponding to an integrated luminosity of about 50 pb^{-1} . Measurements of Standard Model (SM) processes with leptonic final states have previously been published by CMS [5].

Simulated event samples were generated with standard Monte Carlo (MC) programs, including PYTHIA and ALPGEN [6]. The response of the detector was simulated in detail using GEANT [7] and parameterizations of showers and other detector response.

2 Methods

The reconstruction and calibration of electrons and muons follows standard methods [8]. The selection of events is simple, as described in the following sections.

2.1 Electrons

Electrons are reconstructed by associating a cluster in the ECAL with a track. ECAL clusters are formed by associating energy deposits in crystals surrounding a “seed”, locally the highest energy, crystal into collections of crystals [10]. Track reconstruction, which is specific to electrons to allow for bremsstrahlung emission, is seeded from the clusters in the ECAL, firstly by using the cluster energy to search for compatible hits in the pixel detector and then using these hits as seeds to reconstruct a track in the Si tracker. A minimum of 5 hits are required on each track.

Electron candidates must fall within the barrel or endcap fiducial acceptance regions in pseudorapidity of $|\eta| < 1.442$ or $1.560 < |\eta| < 2.5$. The candidate electron is required to deposit most of its energy in the ECAL and relatively little in the HCAL. The energy deposits are also required to have little surrounding calorimeter activity (be isolated) within a cone of $\Delta R < 0.3$ to reject jets. A track isolation criterion is also imposed.

The ECAL was calibrated employing both test beam and pp collision data. A crystal-to-crystal calibration was achieved by requiring a symmetry in the energy deposits in the r - ϕ plan, and electrons from the Z peak were used to set the overall scale [9]. The energy resolution obtained

43 with this dataset is 1.5%.

44 Events are selected in which at least two electron candidates have an $E_t > 25$ GeV. There is no
45 requirement that the electron charges be opposite.

46 2.2 Muons

47 The highly redundant muon system allows the reconstruction of muon tracks independent of
48 the Si tracker. Such “stand-alone” tracks are used to select good Si tracks which can be fitted
49 together with hits in the muon chambers. In order to ensure a good quality measurement, the
50 Si track must have at least 10 hits, and $\chi^2/N_{DF} < 10$. A judicious selection of a subset of the
51 muon chamber hits ensures the best possible muon resolution [11].

52 A pure sample of muons is obtained by demanding consistency of the extrapolated Si track
53 position and the position measured in the muon chambers. Also, the energy registered by the
54 ECAL and HCAL must be consistent with the expectation for a muon of the given energy [12].
55 Non-prompt muons, referred to as “fake” muons here, coming from meson decays are sup-
56 pressed by imposing an isolation requirement based on the sum of the p_T of tracks within a
57 narrow cone centered on the muon.

58 The momentum scale is set using the $Z \rightarrow \mu^+\mu^-$ peak and the known Z boson mass. Given
59 50 pb^{-1} , the relative scale uncertainty is 1.1%. When transferring this calibration to the TeV
60 mass scale, an additional uncertainty of 3% is assigned, accounting for possible non-linear
61 effects. The resolution at high masses is determined by the accuracy of the alignment. At a
62 mass of 1.2 TeV, the resolution is estimated to be 7%, based on studies of residuals.

63 Events are selected which have two isolated muons of opposite charge and $p_T > 20$ GeV.

64 2.3 Efficiency Estimation

65 The efficiency for reconstructing and identifying good lepton candidates is measured using the
66 “tag and probe” approach [13]. A tag lepton is established by applying tight cuts to one lepton;
67 the other candidate is then the probe. Several factors in the overall efficiency are measured,
68 including the trigger efficiency, Si track reconstruction efficiency, and the lepton reconstruction
69 and identification efficiency. For electron and muon pairs, a large sample of high-purity probes
70 is obtained from pairs with an invariant mass compatible with the Z-boson mass. The electron
71 analysis also makes use of pairs from the Drell-Yan tail.

72 Using data from the Z-peak, if the probe object is required only to be a cluster in the ECAL,
73 the efficiency of all subsequent selection criteria is found. Using only a track as the probe
74 object allows the cluster finding efficiency to be estimated. From MC simulations the efficiency
75 of electron identification is found to increase as a function of true energy. This becomes flat
76 beyond about 45 GeV. The total efficiency measured in the data at the Z-pole is $90 \pm 1.7\%$
77 (barrel) and $86.8 \pm 3.8\%$ (endcap). The ratio of the efficiency measured from the data and the
78 efficiency determined from MC simulation at the Z pole is found to be $[YY] \pm 0.017$ (barrel)
79 and $[YYY] \pm 0.038$ (endcap). This scale factor is applied to the efficiency found for electrons
80 with high energies determined from MC simulation to determine the efficiency used for the
81 data sample. The systematic error is obtained by varying the estimated background under the
82 Z peak by 50%. The total trigger efficiency is found to be 100% for events where two electron
83 candidates pass the offline selection criteria.

84 The efficiency was cross checked using the events with an invariant mass greater than 120 GeV.
85 The two methods agree to within statistical errors and efficiencies of $90.5 \pm 1.7\%$ (barrel) and
86 $88.0 \pm 3.8\%$ (endcap) are used throughout this paper.

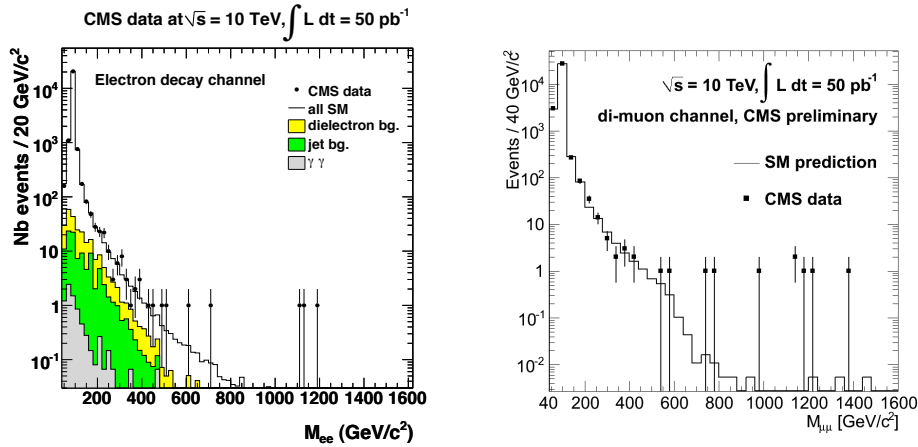


Figure 1: Invariant mass spectra for electrons (*left*) and muons (*right*). The points with error bars represent the CMS data, and the histograms, the predictions based on SM processes.

87 A similar procedure is followed for muons, and using Z-peak data, the overall efficiency is
 88 $97.6 \pm 0.6\%$. There is no sign of a reduction in the efficiency for muon p_T up to about 150 GeV/c,
 89 beyond which there are no events in the data. MC studies indicate that the efficiency remains
 90 constant as a function of p_T to within $\sim 1\%$, which we take as the uncertainty on the efficiency
 91 ratio of high- p_T to moderate- p_T muons.

92 3 Results

93 The compatibility of the data with SM expectations at low di-lepton masses is demonstrated
 94 first, followed by a discussion of the events at high mass.

95 3.1 Yields from SM processes

96 The most prominent contribution to the e^+e^- and $\mu^+\mu^-$ samples comes from the Drell-Yan
 97 process, with additional significant contributions from the $t\bar{t}$, tW , WW , and $Z \rightarrow \tau\tau$ processes.
 98 In addition, jets may be mis-identified as leptons, and contribute to the invariant mass spectra
 99 through QCD multi-jet and vector boson+jet processes. Lastly, di-photon events, where both
 100 photons are mis-reconstructed will contribute to the e^+e^- spectrum.

101 3.1.1 Backgrounds with prompt leptons

102 Non-Drell-Yan backgrounds with prompt leptons are estimated using two complementary
 103 methods. The processes $t\bar{t}$, tW , WW , $Z \rightarrow \tau\tau$ can give rise to any combination of lepton
 104 flavours and a sample of $e\mu$ events is used to estimate the expected e^+e^- and $\mu^+\mu^-$ distribu-
 105 tions. About 10% of the events in this sample come from events in which a jet is mis-identified
 106 as (“fakes”) an electron, mainly in W +jet production, and this is taken into account.

107 The second method applies b -tagging to the di-lepton event sample to estimate the contribution
 108 from top events ($t\bar{t}$ and tW). The b -tagging efficiency is estimated by comparing the number of
 109 single-tagged and double-tagged events, with corrections for acceptance and the contribution
 110 of tW events taken from simulations.

111 The $e\mu$ and the b -tagging estimates are statistically independent, and suffer from different sys-
 112 tematics. Figure 2 shows the agreement of the estimates, indicating that this background con-

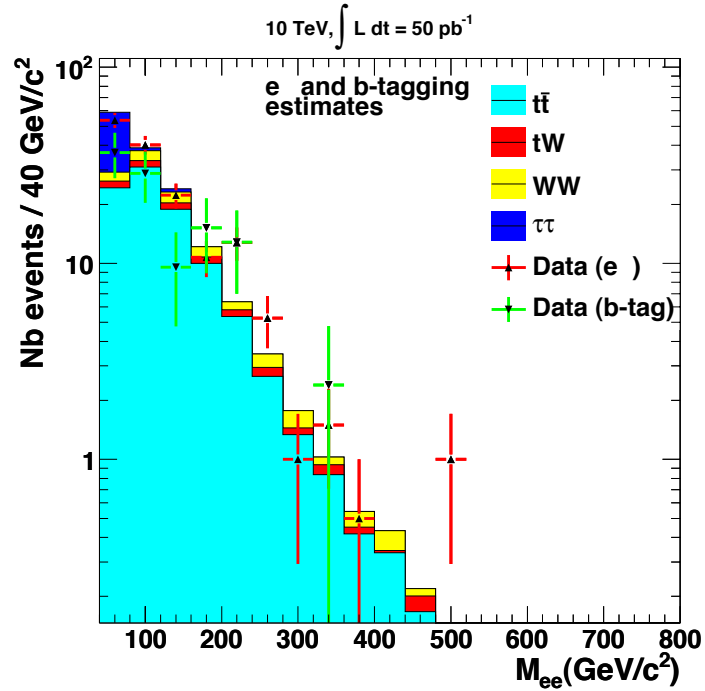


Figure 2: The solid histogram shows the Monte Carlo simulation of the contribution to the di-electron invariant mass spectrum from $t\bar{t}$, tW , WW and $Z \rightarrow \tau\tau$ processes. The red data points result from the $e\mu$ estimation method and the blue from the b-tagging method. The b-tagging method does not estimate contributions from the WW or $Z \rightarrow \tau\tau$ processes.

113 tribution is understood well. Note that $Z \rightarrow \tau\tau$ events contribute to the $e\mu$ estimate only.
 114 The events predominantly contribute outside of the control region between 120-600 GeV. No
 115 correction for this contribution is therefore made to the b -tag estimate of the prompt lepton
 116 background.

117 3.1.2 Fake leptons

118 The probability for a jet to be mis-identified as a lepton has been measured using data samples
 119 obtained with pre-scaled jet triggers. The lowest accessible jet threshold is 30 GeV. The so-called
 120 “fake rate” is computed in bins of E_t or p_T as the numbers of jets passing the lepton selection
 121 requirements divided by the total number of jets. For electrons used in this analysis, the fake
 122 rate is estimated to be $(0.04 \pm 0.01) \times 10^{-3}$ in the barrel and $(0.3 \pm 0.1) \times 10^{-3}$ in the endcap for
 123 a jet with E_t around 200 GeV. For muons, the corresponding number is $(xx \pm yy) \times 10^{-4}$. The
 124 errors are statistical.

125 The mass spectrum of background events with at least one fake lepton is obtained from an
 126 event sample with one object passing all lepton selection criteria, and no other such object.
 127 There must also be a suitable jet. The Drell-Yan contribution to this sample is negligible. The E_t
 128 (p_T) of the jets in this sample are weighted by the fake rate, and the invariant mass is calculated.
 129 This spectrum includes the background from purely multi-jet processes and from a vector boson+jet(s).
 130 A systematic uncertainty of 50% is assigned to account for errors due to converting
 131 jet E_t into electron E_t or muon p_T , and the composition of this sample. The spectrum obtained
 132 is shown in Fig. 1.

133 The di-muon signal sample contains only muon pairs of opposite electric charge; background

134 events with non-prompt muons will contain same-charge pairs which can be used to check the
135 predicted level of such backgrounds. There are 3 events with same-charge muon pairs and
136 $M_{\mu\mu} > 120$ GeV, compared to 2 ± 1 events predicted.

137 3.2 Cosmic Ray Muons

138 The di-muon sample is susceptible to contamination from cosmic ray muons, which can be re-
139 constructed as a pair of oppositely-charged, high-momentum muon tracks. The contribution
140 from cosmic ray muons was estimated using several topological and kinematic criteria, includ-
141 ing the impact parameter, acollinearity, momentum balance, and arrival time of the muon with
142 respect to other tracks in the event. The rate and mass spectrum was established through an
143 analysis of cosmic ray runs (see Ref. [3]), and the number of events in the final sample was esti-
144 mated based on the integrated live time of the experiment during the runs used in the di-muon
145 analysis. For $M_{\mu\mu} > 800$ GeV, the expected number of cosmic ray muon events is less than
146 0.1 event.

147 3.3 di-Lepton Spectra

148 Figure 1 shows the di-lepton mass spectra obtained from CMS data. These are compared the
149 SM expectation based on multi-jet backgrounds estimates directly from the data, and MC simu-
150 lations of other processes. Good agreement is observed for masses below several hundred GeV.

151 Searches for narrow resonances at the Tevatron have placed limits in the mass range 600 GeV
152 to 800 GeV [14]. A control region expected to be free of any new physics signal is defined to be
153 $120 \text{ GeV} < M_{\ell\ell} < 600 \text{ GeV}$, as indicated by the arrow in Fig. 1. The good agreement between
154 the data and the prediction confirms that the SM expectations and the detector performance are
155 well understood. Kolmogorov-Smirnov tests were calculated between the observed spectrum
156 and the prediction; the probabilities are 63% for electrons and 41% for muons.

157 The total number of events observed in this mass range is 421 for the electron channel and
158 478 for the muon channel. The number estimated to come from prompt leptons using the $e\mu$
159 method is 41 ± 3 (stat) ± 7 (syst) (electrons) and 52 ± 8 (muons). The contribution where at least
160 one jet fakes a lepton is measured using the method described above for electrons and is 18 ± 9
161 events. This agrees well with the number of Drell-Yan events expected in this region of $329 \pm$
162 13 (electrons) and 480 ± 17 events for muons, where the error is due to the pdf uncertainty.

163 3.4 Cross Checks

164 The events above 800 GeV are rare, and it is important to check the response of the detector at
165 these scales.

166 3.4.1 ECAL cluster energies

167 The maximum energy deposited in a crystal which is part of the clusters associated with the
168 candidate events close to 1.2 TeV is significantly larger than the energies in the data used for
169 calibration where data originating from Z boson decay, are used. The energy of a 5×5 cluster
170 of crystals can be determined excluding the information from the highest energy crystal and
171 using a knowledge of the lateral shower shape. A precision of between 4-9% is expected using
172 this procedure. Using events with an invariant mass below 600 GeV confirms that this precision
173 is achieved.

174 The cluster energies for the events in the signal region are determined using this procedure and
175 the energies obtained are [we would quote the specific energies here].

Table 1: Kinematic properties of the events displayed in Fig. 3

channel	mass (TeV)	energies (GeV)
e^+e^-	1.18 ± 0.22	780, 330
$\mu^+\mu^-$	1.24 ± 0.41	1244, 812

Table 2: Excesses observed for $M_{\ell\ell} > 800$ GeV. N_{pred} is the predicted number of events from SM processes, including total uncertainty. N_{obs} is the observed number of events.

channel	N_{pred}	N_{obs}	p -value
e^+e^-	0.22 ± 0.10	3	1.5×10^{-3}
$\mu^+\mu^-$	0.36 ± 0.18	6	2.2×10^{-6}
combined	0.58 ± 0.21	9	1.1×10^{-8}

176 3.4.2 Muon chamber signals

177 The properties of the tracks detected in the muon chambers were examined to make sure they
 178 correspond to the expectation for high-energy muons. Similarly, the energies in the ECAL and
 179 HCAL were checked, to exclude the possibility of a high-energy hadron punching through the
 180 calorimetry.

181 Further checks against cosmic ray muons were performed, based on the distribution of the
 182 impact parameter, the acollinearity, and timing of the muon signals with respect to other tracks
 183 in the event. These checks confirm a negligible contribution from cosmic ray muons.

184 3.4.3 Scrutiny of events

185 The individual events with $M_{\ell\ell} > 800$ GeV were scrutinized to check for signs of detector
 186 malfunction or reconstruction errors. **bulk this up**

187 There is no evidence of any defect in the events at high mass.

188 Displays of events from both channels are shown in Fig. 3. Some salient kinematic properties
 189 of these two events are listed in Table 1.

190 3.5 Significance

191 An excess of events is observed in both the e^+e^- and $\mu^+\mu^-$ channels, clustered around 1.2 TeV.
 192 Predictions can be made of the numbers of events with $M_{\ell\ell} > 800$ GeV, based on MC sim-
 193 ulations of SM processes. Table 2 summarizes these predictions, the observations, and the
 194 p -values¹. The combined p -value is 1.1×10^{-8} , corresponding to a 5.7σ significance.

Two scans for narrow resonances were performed over the mass range [800, 2000] GeV in the
 e^+e^- and $\mu^+\mu^-$ channels separately. The signal shape is given by the detector resolution and
 a radiative tail, assuming a negligible total width for the resonance. The negative logarithm
 of the ratio of likelihoods, $\xi = -\ln[\mathcal{L}_{s+b}/\mathcal{L}_b]$, was used as the test statistic, where b refers
 to the background hypothesis and $s + b$ refers to the background plus signal hypothesis; the
 signal is parametrized by a mass and an amplitude. The amplitude (S_{NP}) was parametrized by

¹ Given a mean expected number of events, the p -values is the probability that the number of events observed
 in any one experiment matches or exceeds the number that is observed.

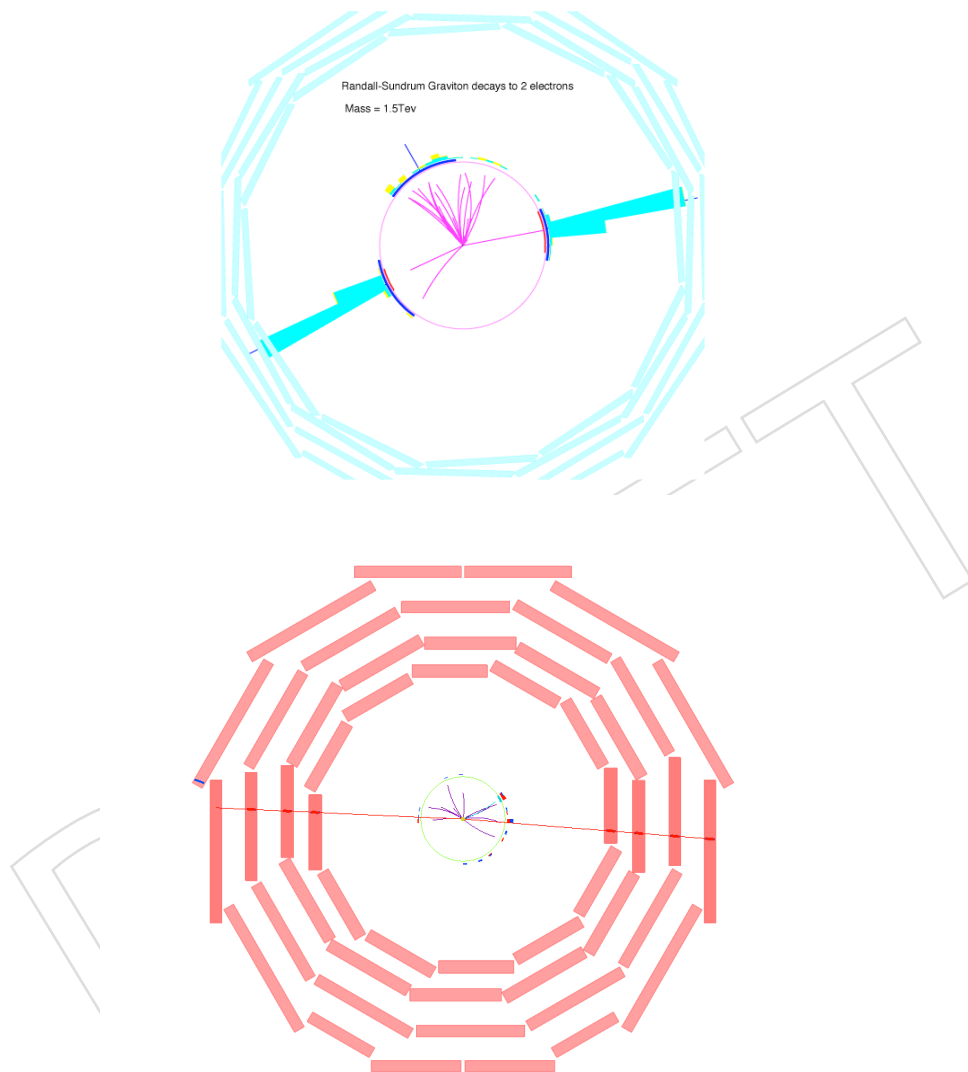


Figure 3: Displays of an e^+e^- event (*top*) and a $\mu^+\mu^-$ event (*bottom*)

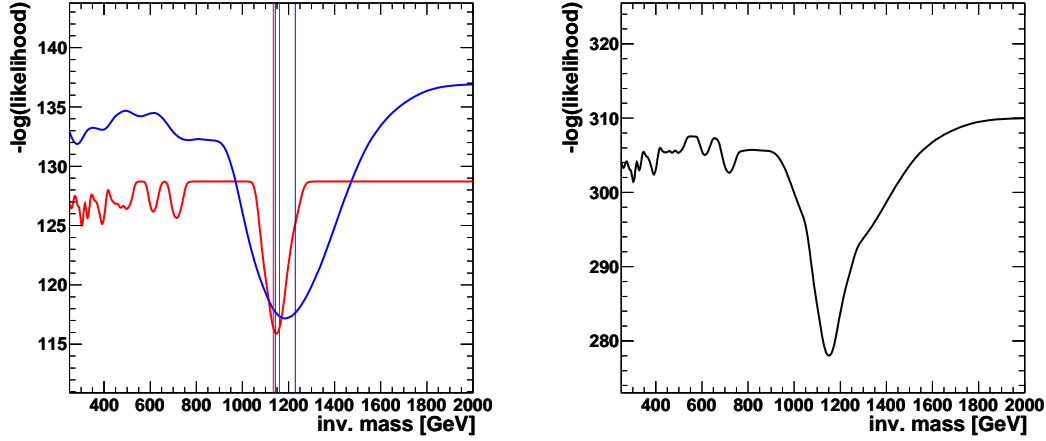


Figure 4: Scans for narrow resonances in the electron and muon channels (*left*), and for both channels combined (*right*).

a number of events (N_{NP}) relative to the number of selected events at the Z-pole (N_Z):

$$S_{\text{NP}} = \left(\frac{N}{A\varepsilon} \right)_{\text{NP}} \cdot \left(\frac{A\varepsilon}{N} \right)_Z. \quad (1)$$

Here, the subscript NP refers to the signal, while Z refers to leptons from the Z peak defined by $60 \text{ GeV} < M_{\ell\ell} < 120 \text{ GeV}$; the ratio of efficiencies was discussed in Section 2.3 and the ratio of acceptances is calculated with MC simulations, with the assumption that the new physics comes from a resonance of spin-1. This amplitude requires no knowledge of the integrated luminosity. The scans are shown in Fig. 4. Evidence for a significant excess is observed near 1.2 TeV in both channels. The probability for observing a statistical fluctuation anywhere in the scanned mass range was taken into account using toy MC tests; the consequent significances are 3.9σ for the electron channel, and 4.9σ for the muon channel.

The largest amplitudes occur near 1.2 TeV in both channels: $S_{\text{NP}}^{ee} = (1.8 \pm 0.3) \times 10^{-3}$ in the e^+e^- channel, and $S_{\text{NP}}^{\mu\mu} = (1.6 \pm 0.4) \times 10^{-3}$ in the $\mu^+\mu^-$ channel. The difference in normalized yields, $\Delta S = S_{\text{NP}}^{ee} - S_{\text{NP}}^{\mu\mu} = (0.2 \pm 0.5) \times 10^{-3}$, is consistent with zero. The probability to observe this value of $|\Delta S|$ or larger is 78%, if the two peaks comes from the same particle, according the MC simulations.

The shape of the test statistic ζ can be used to infer a best value for and uncertainty on the mass. The scans give $M_{ee} = 1.24 \pm 0.02 \pm 0.08 \text{ TeV}$ and $M_{\mu\mu} = 1.19 \pm 0.07 \pm 0.02 \text{ TeV}$, where the first uncertainty is statistical and the second is an estimate of the scale uncertainty. The difference in these values is $\Delta M = M_{ee} - M_{\mu\mu} = 0.05 \pm 0.07 \pm 0.08 \text{ TeV}$. MC simulations show that the probability to observe this value of $|\Delta M|$ or larger is 77%, if the two peaks come from the same particle.

The two measured mass values can be combined using the BLUE method [16], assuming that

the mass peaks come from the same particle. Taking systematic uncertainties into account, the result is

$$M_{\ell\ell} = 1.22 \pm 0.04 \pm 0.08 \text{ TeV}, \quad (2)$$

where the first uncertainty is statistical and the second represents the uncertainties on the mass scales.

A combined scan was performed. The test statistic was based on the product of the likelihoods, and Gaussian constraints on the mass scale uncertainties. The amplitudes were constrained to give the same effective branching ratio for each channel. At each mass the values maximizing the test statistic were found and the right plot in Fig. 4 shows the result of the combined scan. The significance for the combination of electron and muon channels is 6.2σ .

The combined scan yields the amplitude $S_{\text{NP}}^{\ell\ell} = (1.73 \pm 0.14) \times 10^{-3}$. A value for the effective cross section for new physics can be deduced from this value according to $\sigma_{\text{NP}} = \sigma_Z \times S_{\text{NP}}$. Taking $\sigma_Z = 1.87 \pm 0.03 \text{ nb}$ [17] gives

$$\sigma \times B(pp \rightarrow X \rightarrow \ell^+\ell^-) = 21 \pm 3 \pm 2 \pm 1 \text{ pb} \quad (3)$$

where the first uncertainty is statistical, the second includes experimental uncertainties such as the efficiency, and the third reflects the theoretical uncertainties on σ_Z .

It is not possible to make a significant conclusion about the spin of the new resonance on the basis of the current data sample.

4 Conclusion

Evidence for a new narrow resonance has been found in the CMS data corresponding to an integrated luminosity of 50 pb^{-1} taken at a center-of-mass energy of 10 TeV. Narrow peaks are observed near 1.2 TeV in both the e^+e^- and $\mu^+\mu^-$ channels. A combined scan of these channels was used to obtain a mass measurement $M_{\ell\ell} = 1.22 \pm 0.03 \pm 0.08 \text{ TeV}$. The yields support the hypothesis of equal branching ratios. With the assumption that one particle is responsible for both peaks, and that the branching ratios are equal, a cross section $\sigma \times B(pp \rightarrow X \rightarrow \ell^+\ell^-) = 21 \pm 3 \pm 2 \text{ pb}$ has been measured.

Larger data samples will allow more precise measurements of the mass and effective cross section, and to deduce the spin of the new resonance.

Acknowledgments

We thank the technical and administrative staff at CERN and other CMS Institutes, and acknowledge support from: FMSR (Austria); FNRS and FWO (Belgium); CNPq, CAPES, FAPERJ, and FAPESP (Brazil); MES (Bulgaria); CERN; CAS, MoST, and NSFC (China); COLCIENCIAS (Colombia); MSES (Croatia); RPF (Cyprus); Academy of Sciences and NICPB (Estonia); Academy of Finland, ME, and HIP (Finland); CEA and CNRS/IN2P3 (France); BMBF, DFG, and HGF (Germany); GSRT (Greece); OTKA and NKTH (Hungary); DAE and DST (India); IPM (Iran); SFI (Ireland); INFN (Italy); NRF (Korea); LAS (Lithuania); CINVESTAV, CONACYT, SEP, and UASLP-FAI (Mexico); PAEC (Pakistan); SCSR (Poland); FCT (Portugal); JINR (Armenia, Belarus, Georgia, Ukraine, Uzbekistan); MST and MAE (Russia); MSTDS (Serbia); MICINN and CPAN (Spain); Swiss Funding Agencies (Switzerland); NSC (Taipei); TUBITAK and TAEK (Turkey); STFC (United Kingdom); DOE and NSF (USA). Individuals have received

247 support from the Marie-Curie IEF program (European Union); the Leventis Foundation; the A.
248 P. Sloan Foundation; and the Alexander von Humboldt Foundation.

249 References

- 250 [1] a list of good theory reviews
- 251 [2] *CMS Physics Technical Design Report*, CERN/LHCC 2006-001 (2006).
- 252 CMS Collaboration, *The CMS Experiment at the CERN LHC*, Journal of Instrumentation
253 (JINST) **3**, S08004 (2008).
- 254 [3] The volume of CRAFT papers
- 255 [4] CMS uses a traditional coordinate system with the z axis running along the beam, x defin-
256 ing the horizontal coordinate and y defining the vertical. The origin is at the geometric
257 center of the tracker. E_T is the transverse energy of an electron or jet, and p_T is the trans-
258 verse momentum of a track, including muons. The pseudo-rapidity is $\eta = -\ln[\tan(\theta/2)]$.
- 259 [5] list of relevant lepton-based publications from CMS
- 260 [6] standard references to Pythia, Alpgen, and other event generators used in this analysis
- 261 [7] GEANT reference
- 262 [8] references to published papers explaining standard methods for reconstructing and cali-
263 brating electrons and muons.
- 264 [9] reference to ECAL calibration method and measurement
- 265 [10] reference for ECAL crystals and electron reco
- 266 [11] reference for the reco muon cocktail
- 267 [12] Very energetic muons, such as those found here, have a significant probability to interact
268 in the calorimeters. The cut on calorimeter energies is therefore scaled ...
- 269 [13] reference for tag-n-probe methods
- 270 [14] recent Tevatron publications setting limits on narrow resonances
- 271 [15] The expected yields are calculated based on an NNLO cross section calculation: $\sigma =$
272 $xxxx \pm yyyy$ pb. [reference for the SM NLO value for the high-mass DY.]
- 273 [16] reference for the BLUE method of combining measurements
- 274 [17] reference for the SM value for the Z peak (60,120)